Applied Energy 291 (2021) 116857

Contents lists available at ScienceDirect

Applied Energy

journal homepage: www.elsevier.com/locate/apenergy

Coordinated charging and discharging control of electric vehicles to manage supply voltages in distribution networks: Assessing the customer benefit

Nanduni I. Nimalsiri [a,b,*], Elizabeth L. Ratnam [a], Chathurika P. Mediwaththe [a], David B. Smith [a,b], Saman K. Halgamuge [a,c]

[a] School of Engineering, Australian National University, Canberra, ACT 2600, Australia
[b] CSIRO Data61, Eveleigh, NSW 2015, Australia
[c] School of Engineering, University of Melbourne, Parkville, VIC 3010, Australia

ARTICLE INFO

Keywords:
Electric vehicles
Quadratic program
Receding horizon
Supply voltages
Time-of-use
Vehicle-to-grid

ABSTRACT

Increased worldwide uptake of Electric Vehicles (EVs) accentuates the need for developing coordinated EV charging and discharging methods that mitigate detrimental and sustained under-voltage and over-voltage conditions in distribution networks. In this paper, a centrally coordinated EV charge-discharge scheduling method is proposed, referred to as Network-aware EV Charging (and Discharging) N-EVC(D), that takes into account both EV customer economics and distribution grid constraints. Specifically, N-EVC(D) is designed to maintain quasi-steady-state feeder voltages within statutory power quality limits, while minimizing EV customer operational costs associated with: (1) purchasing (or otherwise being compensated for delivering) electricity on a time-of-use tariff; and (2) battery degradation due to frequent charging and discharging. The optimization problem for N-EVC(D) is formulated as a quadratic program, with voltage constraints to limit voltage variability across a radial distribution feeder, and individual EV constraints to satisfy heterogeneous EV charge requirements. In N-EVC(D), each grid-connected EV follows an operator-specified battery schedule that is obtained by solving the proposed quadratic program. A receding horizon implementation is also proposed to support near-real-time N-EVC(D) operations while accommodating non-deterministic EV arrivals and departures. The benefits of N-EVC(D) are assessed by means of numerical simulations carried out on an IEEE test feeder populated with a real-world dataset of residential load collected from households within an Australian distribution network. The simulation results confirm that N-EVC(D) mitigates non-compliant voltage deviations that would otherwise occur when voltage constraints are not enforced. Compared to uncoordinated EV charging, N-EVC(D) offers a 92% – 111% reduction in the operational costs incurred by EV customers.

1. Introduction

The recent dramatic increase in Electric Vehicle (EV) uptake around the globe is enabling a significant reduction in carbon emissions from the transportation sector [1]. However, an adverse consequence of EV proliferation is the increased utilization of electric power grids, potentially exacerbating the risk of supply voltage excursions beyond acceptable power quality limits [2].

The studies in [2] and [3] have revealed that uncoordinated EV charging leads to numerous detrimental electrical grid impacts, including thermal over-loading of transformers, increased power system losses, and significant voltage drops. These voltage drops are particularly pronounced when large numbers of EVs conduct charging simultaneously, mostly upon arrival at home after work. In particular, large voltage deviations reduce the quality of power supplied to consumer electrical appliances, potentially causing misoperation or failure. To deliver high-quality power to end-customers without upgrading existing electrical grid infrastructure, numerous coordinated EV charging approaches have been proposed — as reported in the survey paper [4].

Several authors have proposed optimization-based EV charging methods to address under-voltage conditions coincident with peak power demand [5–15]. By applying a linear approximation to voltage drop within the network, De Hoog et al. [5] formulate a linear optimization problem with the objective of providing as much charging power to the EVs as the network will accommodate. A similar approach is followed in [6] to maximize the total power delivered to EVs, while ensuring the network limits are not exceeded. In [7],

* Corresponding author at: Level 5, 13 Garden Street, Eveleigh, NSW 2015, Australia.
E-mail addresses: nanduni.nimalsiri@anu.edu.au (N.I. Nimalsiri), elizabeth.ratnam@anu.edu.au (E.L. Ratnam), chathurika.mediwaththe@anu.edu.au (C.P. Mediwaththe), david.smith@data61.csiro.au (D.B. Smith), saman.halgamuge@anu.edu.au (S.K. Halgamuge).

https://doi.org/10.1016/j.apenergy.2021.116857
Received 23 December 2020; Received in revised form 16 March 2021; Accepted 18 March 2021
Available online 31 March 2021

a linear program is iteratively solved until voltages fall within the permissible limits. To achieve valley-filling in compliance with the voltage constraints, a shrunken primal–dual subgradient algorithm is proposed in [8], which is later extended in [9] to include a dimension reduction methodology whereby the network topology is partitioned to reduce the complexity. The authors in [10] propose a distributed voltage compensation algorithm to recover voltage violations occurring at distribution nodes. The authors in [11] propose an optimization problem with a variable objective function to improve the voltage profile at the customer Point of Common Coupling (PCC). By contrast, the studies in [12] and [13] investigate methods to control EV charging using local voltage measurements at the PCC. Clement-Nyns et al. [14] minimize distribution system losses under the assumption that mitigating losses will improve the voltage profile. Alternatively, the algorithm in [15] adapts EV charging from voltage-safety-oriented to loss-minimization-oriented, or vice versa, based on EV penetration level. The studies in [16] and [17] propose probabilistic Monte Carlo-based methods to optimize EV charging in a distribution network with renewable power generation, while taking into consideration the minimum voltage allowed for the distribution network.

With the recent introduction of Vehicle-to-Grid (V2G) operation, the management of system voltages within operational limits becomes increasingly challenging, as voltage rise stemming from the reversal of power flow direction must also be addressed. However, with the exceptions of [11] and [14], none of the approaches in [5–17] support V2G operation. Importantly, V2G-based studies that incorporate network constraints together with EV customer economics are less prevalent in the literature [4]. More specifically, the network-aware EV scheduling methods in [5–17] do not consider price-based incentives when charging and discharging EVs. Dong et al. [3] design a pricing scheme for EV fast-charging stations to support voltage control, and Sun et al. [18] propose a cost-minimizing day-ahead charge scheduling approach that regulates network voltages. Bharati and Paudyal [19] propose a hierarchical framework to reduce the cost of EV charging while constraining voltages within the distribution grid. However, all these studies in [3,18,19] assume that EVs do not partake in V2G operation. By contrast, Shekari et al. [20] propose a day-ahead EV scheduling method involving V2G to minimize both network voltage deviations and microgrid operational costs; however, the proposed method does not consider costs associated with the EV customers. Conversely, Crow and others [21] propose an EV scheduling method with V2G to co-optimize customer and system objectives by minimizing both EV charging costs and system load variance; however, the authors do not consider network voltage limitations.

In the literature, many existing approaches, e.g., [7–10,14,19,22], rely on the assumption that EV arrival times are deterministic (known a *priori*), which is not very realistic in general. For example, the algorithm proposed in [22] reduces EV operational costs subject to constraints of EV and power systems; however, day-ahead EV arrival times are required as inputs to the algorithm. Interestingly, the EV charging algorithm in [23] manages EVs with non-deterministic arrivals while minimizing both network voltage deviations and EV charging costs; however, it disregards V2G operation. Numerous receding horizon control approaches are proposed to adapt to various types of uncertainties arising from EV mobility, including stochastic daily trip distances [24], random arrival and departure times [25], and day-ahead forecast errors associated with time-varying load [26] and solar PV estimation [27]. However, these studies in [24–27] do not directly regulate distribution network voltages. Thus, the formulation of an EV charge and discharge scheduling method that minimizes operational costs accrued by EV customers, while circumventing sustained over-voltage and under-voltage conditions, in addition to managing non-deterministic EV arrival and departure times, addresses a significant gap in the existing literature.

In this paper, a Network-aware EV Charging (and Discharging) method called N-EVC(D) is proposed to minimize the operational costs that are accrued to EV customers in the context of time-based financial tariffs, while maintaining feeder nodal voltage magnitudes within prescribed thresholds under quasi-steady-state operating conditions. By supporting both G2V (Grid-to-Vehicle) and V2G operation, N-EVC(D) allows for more efficient utilization of EV idle times (when EVs are parked). To implement N-EVC(D), each EV customer requires to install an energy management system that communicates directly with a Centralized Operator (CO), e.g., an EV aggregator, enabling the CO to coordinate EV battery schedules. The optimization problem for N-EVC(D) is formulated as a Quadratic Program (QP) with the objective of minimizing EV customer related operational costs by: (1) reducing daily payments for electricity received from the grid for EV charging; (2) increasing daily profits from the delivery of electricity to the grid via EV discharging; and (3) reducing excessive EV battery cycling to prolong battery lifespan. In the proposed QP, a network constraint is included to ensure that the voltage delivered to each customer is within the allowable limits at all times. In formulating the respective network constraint, the nodal location of each customer along a radial distribution feeder is specifically taken into account. The proposed QP is also constrained by the requirement to charge all grid-connected EV batteries to their desired State of Charge (SoC) before their specified departure times.

Moreover, this paper combines a receding horizon control approach with N-EVC(D) to manage unexpected connections and disconnections of EVs from the grid. In the proposed Receding Horizon Optimization (RHO)-based N-EVC(D) implementation, the CO repeatedly solves the proposed QP over a moving time horizon and dispatches resultant charge-discharge control sequences to all grid-connected EVs. In summary, the main contributions of this paper are listed as follows.

1. A network-aware EV battery scheduling method called N-EVC(D) is proposed to minimize operational costs associated with EV charging and discharging, while mitigating quasi-steady-state voltage fluctuations falling below a lower voltage limit or exceeding an upper voltage limit.
    - In contrast to the literature focused only on either least-cost EV charging (e.g., [28]) or distribution network congestion management (e.g., [5–15]), N-EVC(D) balances operational costs incurred by EV customers against improvements in supply voltages across the distribution power grid. As such, N-EVC(D) provides benefits to EV customers as well to electrical distributors.
    - N-EVC(D) is formulated as a QP with an objective function that: (1) minimizes EV charging (and discharging) costs in the text of a Time-of-Use (ToU) net metering financial policy as defined in [29], and (2) reduces excessive EV battery degradation caused by frequent charging and discharging.
    - N-EVC(D) leverages a power flow model referred to as the LinDistFlow [30] to capture network power flows and voltages along a radial distribution feeder, wherein each of the EV customers is connected to the wider distribution grid via a PCC, behind which sits a residential power system that consists of an EV and a non-EV load.
    - N-EVC(D) is designed to satisfy all feasible heterogeneous EV charge requirements within the customer-specified time duration.
2. A RHO-based N-EVC(D) algorithm is proposed to accommodate non-deterministic EV arrivals and departures. Specifically, the proposed algorithm supports near-real-time N-EVC(D) control operations as opposed to day-ahead EV charge (and discharge) scheduling, to improve network voltages in the presence of uncertainties including non-deterministic EV arrival times and non-EV load forecast errors.

3. The benefits from N-EVC(D) are assessed via extensive numerical simulations carried out on the IEEE 13 node test feeder using empirical real-life data of residential customers in an Australian distribution network.

The remainder of this paper is organized as follows. In Section 2, the residential power system associated with a single EV customer is introduced. In Section 3, the N-EVC(D) method is proposed to coordinate EV charge and discharge schedules, considering an EV population distributed across a medium voltage distribution network. In Section 4, the numerical simulation results are presented, followed by the Conclusion in Section 5.

Notation

Let $\mathbb{R}^{\ell}$ denote ℓ-dimensional vectors of real numbers and $\mathbb{R}^{\ell}_{\geq 0}$ denote ℓ-dimensional vectors with all non-negative components, where, as usual, $\mathbb{R}^1 = \mathbb{R}$. For a vector or matrix $\boldsymbol{A}$, its transpose is denoted by $\boldsymbol{A}^{\top}$. $\mathbf{0}$ denotes the all-zero column vector of length ℓ and $\mathbf{I}$ denotes the ℓ-by-ℓ identity matrix. $\mathbf{1}$ denotes an all-ones column vector, where the context will make clear the dimension intended. For two matrices $\boldsymbol{A} = [a_{ij}] \in \mathbb{R}^{m\times n}$ and $\boldsymbol{B} = [b_{ij}] \in \mathbb{R}^{p\times q}$, $\boldsymbol{A} \oplus \boldsymbol{B} = [c_{ij}] \in \mathbb{R}^{(m+p)\times(n+q)}$ denotes the matrix satisfying $c_{ij} = a_{ij}$ when $i \leq m$ and $j \leq n$, $c_{ij} = b_{(i-m)(j-n)}$ when $i > m$ and $j > n$, and $c_{ij} = 0$ elsewhere, i.e, $\boldsymbol{A} \oplus \boldsymbol{B} = \text{diag}(\boldsymbol{A}, \boldsymbol{B})$. For two sets $\mathcal{P}$ and $\mathcal{Q}$, $\mathcal{P} \cap \mathcal{Q}$ denotes the set that has only elements common to both $\mathcal{P}$ and $\mathcal{Q}$.

2. Preliminaries

This paper considers EV charge and discharge scheduling in a distribution network serving a set of customers (e.g., residential and small business customers) denoted by $\mathbb{H} := \{1, \dots, n, \dots, h\}$. The set of customers is divided into two subsets $\mathbb{H}_1$ and $\mathbb{H}_2$, i.e., $\mathbb{H} = \mathbb{H}_1 \cup \mathbb{H}_2$, where $\mathbb{H}_1$ consists of customers with *gridable EVs* that can both charge and discharge from or to the electric grid, and $\mathbb{H}_2$ consists of customers with *charge-only EVs*.

A planning time-horizon $[0, T]$ is considered that is discretized into ℓ time intervals of temporal resolution Δ. Let $\mathbb{S} := \{1, \dots, t, \dots, \ell\}$, whereby a time interval is denoted by $((t-1)\Delta, t\Delta)$ for all $t \in \mathbb{S}$. In this paper, T and Δ are set to $T = 24$ h and $\Delta = 0.5$ h, such that $\ell = T/\Delta = 48$. Other choices are certainly possible, subject only to commensurability of T, ℓ and Δ.

Fig. 1 illustrates the assumed topology of a *residential power system* corresponding to customer $n \in \mathbb{H}$, where the EV belonging to customer n is labeled as EV_n. Bi-directional smart meter **M** measures and records power flow $y_n(t)$ (in kW), where the measured power flow from (to) the grid to (from) the residential power system of customer n over the period $\big((t-1)\Delta, t\Delta\big)$ is represented by $y_n(t) \in \mathbb{R}_{\geq 0}$ ($y_n(t) \in \mathbb{R}_{<0}$) for all $t \in \mathbb{S}$. Accordingly, the *grid power profile* of customer n over the period $[0, T]$ is defined by $\boldsymbol{y}_n := [y_n(1), \dots, y_n(t), \dots, y_n(\ell)]^{\top} \in \mathbb{R}^{\ell}$. Throughout the paper, EV-indices are sub-scripted and time-indices are parenthesized.

Next, the residential power consumption (or excess renewable power generation) of customer n over the period $\big((t-1)\Delta, t\Delta\big)$ is represented by $z_n(t) \in \mathbb{R}_{\geq 0}$ ($z_n(t) \in \mathbb{R}_{<0}$) (in kW) for all $t \in \mathbb{S}$. In more detail, $z_n(t) \geq 0$ when power is delivered to the non-EV load and $z_n(t) < 0$ when the non-EV load generates excess power (e.g., rooftop solar generation is in excess of the non-EV load power consumption). Accordingly, the day-ahead *non-EV load profile* of customer n over the period $[0, T]$ is defined by $\boldsymbol{z}_n := [z_n(1), \dots, z_n(t), \dots, z_n(\ell)]^{\top} \in \mathbb{R}^{\ell}$. Likewise, the power flow delivered to (from) EV_n (in kW) over the period $\big((t-1)\Delta, t\Delta\big)$ is represented by $x_n(t) \in \mathbb{R}_{\geq 0}$ ($x_n(t) \in \mathbb{R}_{<0}$) for all $t \in \mathbb{S}$, and the *battery profile* of EV_n over the period $[0, T]$ is defined by $\boldsymbol{x}_n := [x_n(1), \dots, x_n(t), \dots, x_n(\ell)]^{\top} \in \mathbb{R}^{\ell}$. By convention, charge rates are positive ($x_n(t) > 0$) and discharge rates are negative ($x_n(t) < 0$).

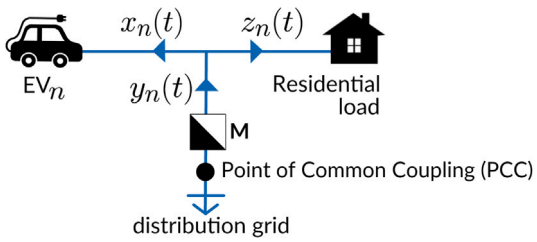

Fig. 1. Residential power system for customer $n \in \mathbb{H}$, illustrating the electrical path from EV_n to the wider distribution grid. The Point of Common Coupling (PCC), which is unique for each customer, represents the point where the customer connects to the distribution grid. Arrows associated with $x_n(t)$, $z_n(t)$ and $y_n(t)$ illustrate the assumed direction of positive power flow, where $t \in \mathbb{S}$. Bidirectional meter **M** measures and records power flow $y_n(t)$. For simplicity, reactive power flows (in kVAR) are not shown in the figure.

From the configuration of the residential power system in Fig. 1, the following power balance equation must hold for all $t \in \mathbb{S}$.

$$y_n(t) := z_n(t) + x_n(t) \tag{1}$$

According to Eq. (1), the grid power profile reduces to the non-EV load profile (i.e., $\boldsymbol{y}_n = \boldsymbol{z}_n$) in the absence of an EV in Fig. 1. Each EV_n ($n \in \mathbb{H}$) has a set of arbitrary parameters that include the arrival time index $a_n \in \mathbb{S}$, intended departure time index $d_n \in \mathbb{S}$, battery capacity σ_n (in kWh), initial SoC $\hat{u}_n$ (in kWh), target SoC $\ddot{u}_n$ (in kWh), minimum SoC $\underline{u}_n$ (in kWh), maximum SoC $\overline{u}_n$ (in kWh), maximum charge rate $\overline{x}_n$ (in kW), maximum discharge rate $\underline{x}_n$ (in kW), charge efficiency $\overline{\mu}_n$ ($0 \leq \overline{\mu}_n \leq 1$) and discharge efficiency $\underline{\mu}_n$ ($\underline{\mu}_n \geq 1$). Here, a_n and d_n are within the day-ahead time horizon $[0, T]$, and extensions to adapt the time horizon accommodating later departure times are straightforward.

Let $\Lambda_n := \{a_n \in \mathbb{R}_{\geq 0}, d_n \in \mathbb{R}_{>0}, \sigma_n \in \mathbb{R}_{>0}, \hat{u}_n \in \mathbb{R}_{\geq 0}, \ddot{u}_n \in \mathbb{R}_{\geq 0}, \underline{u}_n \in \mathbb{R}_{\geq 0}, \overline{u}_n \in \mathbb{R}_{>0}, \overline{x}_n \in \mathbb{R}_{\geq 0}, \underline{x}_n \in \mathbb{R}_{\leq 0}, \overline{\mu}_n \in \mathbb{R}_{\geq 0}, \underline{\mu}_n \in \mathbb{R}_{>0}\}$, where Λ_n denotes the *charging specification* for EV_n ($n \in \mathbb{H}$) [31]. For customers in $\mathbb{H}_2$ with charge-only EVs, by definition $\underline{x}_n = 0$. The initial SoC $\hat{u}_n$ is obtained from the EV battery management system. Upon arrival at home, the EV owner must specify an expected departure time index d_n and a target SoC $\ddot{u}_n$ that is feasible to reach before the expected departure time, i.e., the condition $\ddot{u}_n \leq \hat{u}_n + (d_n - a_n)\overline{\mu}_n\, \overline{x}_n \Delta$ must hold for $n \in \mathbb{H}$. For each EV_n ($n \in \mathbb{H}$), the SoC (in kWh) of battery at time $t\Delta$ is denoted by $u_n(t)$, where

$$u_n(t) := \hat{u}_n + \Delta \sum_{j=1}^{t} x_n(j)\mu_n(j) \tag{2}$$

with $\mu_n(j) = \overline{\mu}_n$ if $x_n(j) \geq 0$ and $\mu_n(j) = \underline{\mu}_n$ otherwise. Accordingly, the *SoC profile* of EV_n ($n \in \mathbb{H}$) is defined as $\boldsymbol{u}_n := [u_n(1), \dots, u_n(t), \dots, u_n(\ell)]^{\top} \in \mathbb{R}^{\ell}_{\geq 0}$. Eq. (2) employs the battery model in [8], however, more specific battery models as in [32] can be similarly considered.

In minimizing the EV operational cost associated with purchasing and delivering electricity, a ToU pricing scheme is considered, which is fixed by the utility or an energy retailer [33]. The daily variations of electricity price are represented by the *pricing profile* $\boldsymbol{\eta} := [\eta(1), \dots, \eta(t), \dots, \eta(\ell)]^{\top} \in \mathbb{R}^{\ell}_{\geq 0}$, where $\eta(t)$ is the price of electricity (in \$/kWh) over the time period $\big((t-1)\Delta, t\Delta\big)$. Along with ToU tariffs, this paper employs a financial policy of *net metering*, the defining characteristic of which is that each customer is billed at the same rate as they are compensated for delivering power to the grid [34]. Accordingly, the energy bill (in \$) for customer $n \in \mathbb{H}$ is defined by $\Delta\boldsymbol{\eta}^{\top}\boldsymbol{y}_n := \Delta\boldsymbol{\eta}^{\top}\boldsymbol{z}_n + \Delta\boldsymbol{\eta}^{\top}\boldsymbol{x}_n$, where $\Delta\boldsymbol{\eta}^{\top}\boldsymbol{z}_n$ is a nondeferrable cost related to non-EV power consumption (or excess generation) and $\Delta\boldsymbol{\eta}^{\top}\boldsymbol{x}_n$ is a deferrable cost related to EV charging and discharging.

3. Problem formulation

First, an optimization problem in the form of a QP is formulated to schedule charging and discharging of a single EV that is connected to the electric power grid via the residential power system illustrated in Fig. 1. Next, the N-EVC(D) method is proposed, wherein the former QP is extended to include a voltage constraint, which couples charge-discharge rates of all EVs across a distribution feeder. Lastly, a receding horizon implementation for N-EVC(D) is also proposed.

3.1. EV battery constraints

The problem of scheduling each $\text{EV}_n (n \in \mathbb{H})$ involves a set of constraints as detailed below. To limit the occurrence of over-charging or over-discharging, the safety constraint $\underline{u}_n \le u_n(t) \le \overline{u}_n$ is introduced, such that the SoC profile $\boldsymbol{u}_n$ is constrained by

$$\underline{u}_n \mathbf{1} \le \boldsymbol{u}_n \le \overline{u}_n \mathbf{1}. \tag{3}$$

To simplify the notation, let $\underline{\sigma}_n := (\underline{u}_n - \hat{u}_n)/\Delta$ and $\overline{\sigma}_n := (\overline{u}_n - \hat{u}_n)/\Delta$. Then (2) and (3) can be combined as

$$\underline{\sigma}_n \mathbf{1} \le \mathbf{T}\boldsymbol{x}_n \le \overline{\sigma}_n \mathbf{1}, \tag{4}$$

where $\mathbf{T} = [t_{ij}] \in \mathbb{R}^{\ell \times \ell}$ denotes a matrix satisfying $t_{ij} = \mu_n(j)$ for $i \ge j$ and $t_{ij} = 0$ elsewhere. To accommodate limits on EV battery charge-discharge rates, the constraint $\underline{x}_n \le x_n(t) \le \overline{x}_n$ is introduced for all $t \in \mathbb{S}$, such that the battery profile $\boldsymbol{x}_n$ is constrained by

$$\underline{x}_n \mathbf{1} \le \boldsymbol{x}_n \le \overline{x}_n \mathbf{1}. \tag{5}$$

Considering the initial SoC and the target SoC of the EV battery, the energy requirement for $\text{EV}_n (n \in \mathbb{H})$ can be expressed as $e_n := \ddot{u}_n - \hat{u}_n$ (in kWh). To accommodate the respective charging demand ahead of an expected departure time, the constraint $u_n(\ell) = \ddot{u}_n$ is enforced, which when combined with (2) yields

$$\mathbf{1}^\top \boldsymbol{x}_n = e_n/\Delta. \tag{6}$$

An EV is available for charging (or discharging) only between its arrival and departure times. To constrain the EV charging and discharging time duration, a diagonal matrix $\boldsymbol{\mathcal{L}}_n = [l_{ij}] \in \mathbb{R}^{\ell \times \ell}$ is defined, in which the i^{th} $(1 \le i \le \ell)$ diagonal entry is 1 if the EV is available across time interval $\big((i-1)\Delta, i\Delta\big)$, and 0 if the EV is not available across time interval $\big((i-1)\Delta, i\Delta\big)$. More specifically, if $i = j$ and $a_n < i \le d_n$, then $l_{ij} = 1$, otherwise $l_{ij} = 0$. Clearly, if $i \ne j$ then $l_{ij} = 0$. Consequently, the battery profile $\boldsymbol{x}_n$ is further constrained by

$$(\mathbf{I} - \boldsymbol{\mathcal{L}}_n)\boldsymbol{x}_n = \mathbf{0}. \tag{7}$$

3.2. Minimizing operational costs

The *operational cost* (in \$/day) incurred by EV customer $n \in \mathbb{H}$ is denoted by $\Omega_n(\boldsymbol{x}_n)$, and it is defined as the sum of two cost components: (1) the time-varying cost of purchasing energy for EV charging (and the time-varying profit from delivering energy via EV discharging), and (2) the cost of EV battery degradation. Here, a financial policy of net-metering is assumed in the context of an EV customer purchasing and delivering electricity. The combined operational cost for EV customer $n \in \mathbb{H}$ is then defined by

$$\Omega_n(\boldsymbol{x}_n) := \sum_{t=1}^{\ell} \big(\Delta\eta(t)x_n(t) + \alpha_n x_n(t)^2\big), \tag{8}$$

where α_n is a regularization constant that is introduced to yield a smoother battery profile $\boldsymbol{x}_n$, avoiding unnecessary charging and discharging, or otherwise, reducing the number of charge-discharge cycles. The first term in (8) represents the energy bill attributed to EV charging (and discharging). The second term in (8), previously used in [35], is considered a proxy for the battery degradation cost, which can be alternatively represented by other cost functions as presented in [36].

By combining EV charge and discharge rates with prices for buying and selling electricity, it can be determined if the customer incurs an energy bill, or rather, is compensated. In other words, when $\Omega_n(\boldsymbol{x}_n) > 0$, there exists a *financial cost* from charging and discharging the EV battery, whereas when $\Omega_n(\boldsymbol{x}_n) < 0$, there exists a *financial benefit* from charging and discharging the EV battery. To minimize the operational cost $\Omega_n(\boldsymbol{x}_n)$ for each EV $n \in \mathbb{H}$, the following Lemma is proposed.

Lemma 1 (*QP-1*). *Consider a financial policy of net metering, with $\boldsymbol{\eta} \in \mathbb{R}^{\ell}_{\ge 0}$ assumed fixed and known. The minimization of expression (8), subject to EV battery constraints (4)–(7), can be succinctly written as the following QP:*

$$\min_{\boldsymbol{x}_n \in \mathbb{R}^{\ell}} \boldsymbol{c}^\top \boldsymbol{x}_n + \boldsymbol{x}_n^\top \boldsymbol{H}_n \boldsymbol{x}_n \tag{9a}$$

subject to

$$\boldsymbol{A}_n \boldsymbol{x}_n \ge \boldsymbol{b}_n \tag{9b}$$

$$\bar{\boldsymbol{A}}_n \boldsymbol{x}_n = \bar{\boldsymbol{b}}_n, \tag{9c}$$

where

$$\begin{aligned}
\boldsymbol{x}_n &:= \big[\, x_n(1), \dots x_n(t), \dots x_n(\ell) \,\big]^\top && \in \mathbb{R}^{\ell}, \\
\boldsymbol{H}_n &:= \alpha_n \mathbf{I} && \in \mathbb{R}^{\ell \times \ell}, \\
\boldsymbol{c} &:= \Delta\boldsymbol{\eta} && \in \mathbb{R}^{\ell}, \\
\boldsymbol{A}_n &:= \big[\, \mathbf{I} \quad -\mathbf{I} \quad \mathbf{T}^\top \quad -\mathbf{T}^\top \,\big]^\top && \in \mathbb{R}^{4\ell \times \ell}, \\
\bar{\boldsymbol{A}}_n &:= \big[\, \mathbf{1} \quad (\mathbf{I} - \boldsymbol{\mathcal{L}}_n) \,\big]^\top && \in \mathbb{R}^{(\ell+1) \times \ell}, \\
\boldsymbol{b}_n &:= \big[\, \underline{x}_n \mathbf{1}^\top \quad -\overline{x}_n \mathbf{1}^\top \quad \underline{\sigma}_n \mathbf{1}^\top \quad -\overline{\sigma}_n \mathbf{1}^\top \,\big]^\top && \in \mathbb{R}^{4\ell}, \\
\bar{\boldsymbol{b}}_n &:= \big[\, e_n/\Delta \quad \mathbf{0}^\top \,\big]^\top && \in \mathbb{R}^{\ell+1}.
\end{aligned}$$

Proof. The objective function (9a) minimizes the operational cost for EV customer $n \in \mathbb{H}$, which is defined as $\Omega_n(\boldsymbol{x}_n)$ in (8). For EV_n, constraint (9b) combines inequality constraints (4) and (5), and constraint (9c) combines equality constraints (6) and (7). ■

Throughout, the process of a customer $n \in \mathbb{H}_1$ implementing the battery profile returned by QP-1 is referred to as *Price-based EV Charging-Discharging (P-EVCD)*, and the process of a customer $n \in \mathbb{H}_2$ implementing the battery profile returned by QP-1 is referred to as simply *Price-based EV Charging (P-EVC)*. In the assessment of the network and customer benefits, P-EVC(D) serves as a benchmark against the N-EVC(D) method proposed in this paper, which is an extension of QP-1 to alleviate over-voltage and under-voltage conditions arising from P-EVC(D).

3.3. Network-aware EV battery scheduling

A single-phase, radial distribution network is considered that is represented by a graph $\mathcal{G} = \{\mathcal{V}, \mathcal{E}\}$, where $\mathcal{V} = \{0, \dots, g, \dots, k\}$ is the set of vertices representing the nodes along the distribution feeder, and $\mathcal{E} \subseteq \mathcal{V} \times \mathcal{V}$ is the set of edges representing the distribution lines spanning the nodes of the distribution feeder. The edge between two adjacent nodes $i \in \mathcal{V}$ and $j \in \mathcal{V}$ is denoted by $(ij) \in \mathcal{E}$, with node i lying between node 0 and node j. Graph $\mathcal{G}$ is assumed to be simple with no repeated edges or self loops for any vertex $g \in \mathcal{V}$, i.e., $(gg) \notin \mathcal{E}$. Furthermore, graph $\mathcal{G}$ is assumed to be a rooted tree, where root vertex is the feeder head represented by node 0. That means, for every vertex $g \in \mathbb{V}$, where $\mathbb{V} = \mathcal{V} \setminus \{0\} = \{1, \dots, g, \dots, k\}$, there is a unique path from root node 0 to node g, and the set of edges on the unique path from node 0 to node $g \in \mathbb{V}$ is denoted by $\mathcal{E}^g \subseteq \mathcal{E}$. Throughout, node-indices are super-scripted.

Each node $g \in \mathbb{V}$ connects N^g number of residential power systems (shown in Fig. 1), such that $N^g \ge 0$ and $\sum_{g=1}^{k} N^g = h$. For example, in the distribution network depicted in Fig. 2, $k = 12$, and all nodes in

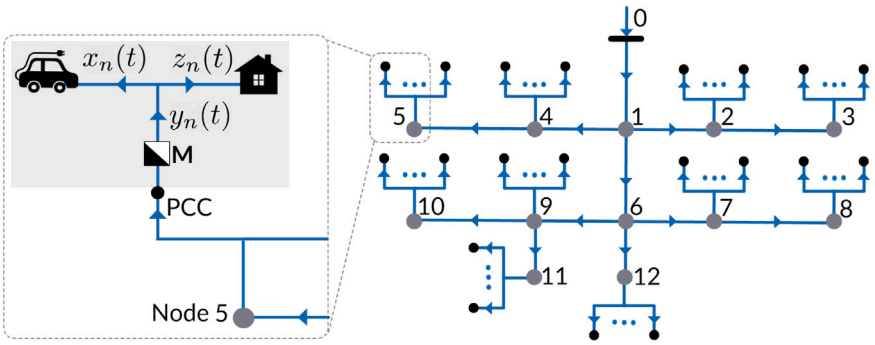

Fig. 2. A radial distribution feeder connecting N^g residential power systems at each node $g \in \mathbb{V}$. Arrows associated with edges in $\mathcal{E}$ illustrate the assumed direction of positive power flow. Left: node 5 is zoomed in for a more detailed representation.

$\mathbb{V}$ except nodes 1 and 6 have one or more residential power systems connected. In Fig. 2, the customer index is initialized as $n = 1$ at node 2, and then n is incremented through all customers connected to node 2, and then through all customers across subsequent nodes $g \in \mathbb{V}$, in ascending order, respectively.

Let $\boldsymbol{\Upsilon} \in \mathbb{R}^{k\times h}_{\geq 0}$ be a matrix specifying the connectivity of customers $n \in \mathbb{H}$ across different nodes $g \in \mathbb{V}$ (i.e, nodal location) along the distribution feeder. For each node $g \in \mathbb{V}$, let $\boldsymbol{\Upsilon}^g = \mathbf{1}^\top \in \mathbb{R}^{1\times N^g}_{\geq 0}$, such that

$$\boldsymbol{\Upsilon} := \oplus_{g=1}^{k} \boldsymbol{\Upsilon}^g \in \mathbb{R}^{k\times h}_{\geq 0}. \tag{10}$$

In what follows, the voltage magnitude at each node $g \in \mathbb{V}$ is approximated using the *LinDistFlow* (linearized Distflow [37]) equations that are proposed in [30]. The LinDistFlow equations are widely exploited and justified in the power systems literature on optimal power flow control of distributed energy resources in radial distribution networks [38].

Let $|v^0|$ denote the voltage magnitude at root node 0, which is set to the nominal voltage, i.e., $|v^0| = 1$ per unit (p.u.). Let $|v^g(t)|$ denote the voltage magnitude at node g at time $t\Delta$. Let $p^g(t) \in \mathbb{R}_{\geq 0}$ ($p^g(t) \in \mathbb{R}_{<0}$) denote the real power (in kW) consumed (injected) at node g over the period $\big((t-1)\Delta, t\Delta\big)$, and $q^g(t) \in \mathbb{R}_{\geq 0}$ ($q^g(t) \in \mathbb{R}_{<0}$) denote the reactive power (in kVAR) consumed (injected) at node g over the period $\big((t-1)\Delta, t\Delta\big)$. Let r^{ij} and x^{ij} $(i, j \in \mathcal{V})$ denote the resistance and reactance of edge $(ij) \in \mathcal{E}$, respectively. Furthermore, let $\boldsymbol{R} \in \mathbb{R}^{k\times k}_{\geq 0}$ and $\boldsymbol{X} \in \mathbb{R}^{k\times k}_{\geq 0}$ denote two positive definite matrices [39] in which the elements corresponding to g^{th} row and $\hat{g}^{\text{th}}$ column are $R^{g\hat{g}}$ and $X^{g\hat{g}}$, respectively. Next, the following are defined:

$$\boldsymbol{V}^0 := \big[\ |v^0|^2, \dots, |v^0|^2, \dots, |v^0|^2\ \big]^\top \in \mathbb{R}^k, \tag{11a}$$
$$\boldsymbol{V}(t) := \big[\ |v^1(t)|^2, \dots, |v^g(t)|^2, \dots, |v^k(t)|^2\ \big]^\top \in \mathbb{R}^k, \tag{11b}$$
$$\boldsymbol{P}(t) := \big[\ p^1(t), \dots, p^g(t), \dots, p^k(t)\ \big]^\top \in \mathbb{R}^k, \tag{11c}$$
$$\boldsymbol{Q}(t) := \big[\ q^1(t), \dots, q^g(t), \dots, q^k(t)\ \big]^\top \in \mathbb{R}^k, \tag{11d}$$
$$R^{g\hat{g}} := \textstyle\sum_{(ij)\in(\mathcal{E}^g\cap\mathcal{E}^{\hat{g}})} r^{ij} \in \mathbb{R}, \tag{11e}$$
$$X^{g\hat{g}} := \textstyle\sum_{(ij)\in(\mathcal{E}^g\cap\mathcal{E}^{\hat{g}})} x^{ij} \in \mathbb{R}. \tag{11f}$$

Then the LinDistFlow equation can be written as

$$\boldsymbol{V}(t) := \boldsymbol{V}^0 - 2\boldsymbol{R}\boldsymbol{P}(t) - 2\boldsymbol{X}\boldsymbol{Q}(t). \tag{12}$$

Next, the power flows at a single node $g \in \mathbb{V}$ are described in more detail. Recall, node g is connected to N^g number of customers and therefore the net real and reactive power consumption (or injection) at node g is determined by the total power consumption (and injection) of all EV and non-EV loads associated with those set of customers. The net real power (in kW) consumed (or injected) by all non-EV loads connected to node $g \in \mathbb{V}$ over the period $\big((t-1)\Delta, t\Delta\big)$ is denoted by $\widetilde{p}^g(t) \in \mathbb{R}_{\geq 0}$ ($\widetilde{p}^g(t) \in \mathbb{R}_{<0}$), for all $t \in \mathbb{S}$, and the net reactive power (in kVAR) consumed (or injected) by all non-EV loads connected to node $g \in \mathbb{V}$ over the period $\big((t-1)\Delta, t\Delta\big)$ is denoted by $\widetilde{q}^g(t) \in \mathbb{R}_{\geq 0}$ ($\widetilde{q}^g(t) \in \mathbb{R}_{<0}$), for all $t \in \mathbb{S}$. Similarly, the real power (in kW) consumed (or injected) by all EVs connected to node $g \in \mathbb{V}$ over the period $\big((t-1)\Delta, t\Delta\big)$ is denoted by $\widehat{p}^g(t) \in \mathbb{R}_{\geq 0}$ ($\widehat{p}^g(t) \in \mathbb{R}_{<0}$), for all $t \in \mathbb{S}$, and the reactive power (in kVAR) consumed (or injected) by all EVs connected to node g over the period $\big((t-1)\Delta, t\Delta\big)$ is denoted by $\widehat{q}^g(t) \in \mathbb{R}_{\geq 0}$ ($\widehat{q}^g(t) \in \mathbb{R}_{<0}$), for all $t \in \mathbb{S}$. By ignoring losses over the period $\big((t-1)\Delta, t\Delta\big)$, $p^g(t)$ and $q^g(t)$ can be expressed as

$$p^g(t) := \widetilde{p}^g(t) + \widehat{p}^g(t), \quad q^g(t) := \widetilde{q}^g(t) + \widehat{q}^g(t) \tag{13}$$

for all $t \in \mathbb{S}$ and $g \in \mathbb{V}$. Next, the following vectors are defined:

$$\widetilde{\boldsymbol{P}}(t) := \big[\ \widetilde{p}^1(t), \dots, \widetilde{p}^g(t), \dots, \widetilde{p}^k(t)\ \big]^\top \in \mathbb{R}^k, \tag{14}$$
$$\widetilde{\boldsymbol{Q}}(t) := \big[\ \widetilde{q}^1(t), \dots, \widetilde{q}^g(t), \dots, \widetilde{q}^k(t)\ \big]^\top \in \mathbb{R}^k, \tag{15}$$
$$\widehat{\boldsymbol{P}}(t) := \big[\ \widehat{p}^1(t), \dots, \widehat{p}^g(t), \dots, \widehat{p}^k(t)\ \big]^\top \in \mathbb{R}^k, \tag{16}$$
$$\widehat{\boldsymbol{Q}}(t) := \big[\ \widehat{q}^1(t), \dots, \widehat{q}^g(t), \dots, \widehat{q}^k(t)\ \big]^\top \in \mathbb{R}^k, \tag{17}$$

such that $\boldsymbol{P}(t) = \widetilde{\boldsymbol{P}}(t) + \widehat{\boldsymbol{P}}(t)$ and $\boldsymbol{Q}(t) = \widetilde{\boldsymbol{Q}}(t) + \widehat{\boldsymbol{Q}}(t)$ for all $t \in \mathbb{S}$. Let $\widetilde{\boldsymbol{V}}(t) := 2\boldsymbol{R}\widetilde{\boldsymbol{P}}(t) + 2\boldsymbol{X}\widetilde{\boldsymbol{Q}}(t) \in \mathbb{R}^k$, where $\widetilde{\boldsymbol{V}}(t)$ represents the voltage drop caused by non-EV loads connected to the distribution feeder at time $t\Delta$. By way of the linearity of Eq. (12), it can be obtained that

$$\boldsymbol{V}(t) := \boldsymbol{V}^0 - \widetilde{\boldsymbol{V}}(t) - \big(2\boldsymbol{R}\widehat{\boldsymbol{P}}(t) + 2\boldsymbol{X}\widehat{\boldsymbol{Q}}(t)\big). \tag{18}$$

Let $\boldsymbol{\mathcal{V}}(t) := \boldsymbol{V}^0 - \widetilde{\boldsymbol{V}}(t) \in \mathbb{R}^k$ denote the *baseline voltages* at time $t\Delta$, where g^{th} element in vector $\boldsymbol{\mathcal{V}}(t)$ represents the squared voltage magnitude of node $g \in \mathbb{V}$ when there are no EVs grid-connected to the distribution feeder at time $t\Delta$. As proposed in [8], it is considered that EVs charge (and discharge) real power (in kW) only. That is, $\widehat{q}^g(t) = 0$ for all $t \in \mathbb{S}$ and for all $g \in \mathbb{V}$, implying $\widehat{\boldsymbol{Q}}(t) = \mathbf{0}$. Substituting $\boldsymbol{\mathcal{V}}(t)$ and $\widehat{\boldsymbol{Q}}(t)$ in Eq. (18) yields

$$\boldsymbol{V}(t) := \boldsymbol{\mathcal{V}}(t) - 2\boldsymbol{R}\widehat{\boldsymbol{P}}(t). \tag{19}$$

Let $\boldsymbol{\mathcal{X}}(t) := \big[\ x_1(t), \dots, x_n(t), \dots, x_h(t)\ \big]^\top \in \mathbb{R}^h$, where the n^{th} element in $\boldsymbol{\mathcal{X}}(t)$ represents the charge (or discharge) rate of $\text{EV}_n (n \in \mathbb{H})$ at time $t\Delta$. Then, using the definitions in Eqs. (10) and (16), it can be derived that

$$\widehat{\boldsymbol{P}}(t) := \boldsymbol{\Upsilon}\boldsymbol{\mathcal{X}}(t), \tag{20}$$

for all $t \in \mathbb{S}$. Let $\boldsymbol{\mathcal{D}} := -2\boldsymbol{R}\boldsymbol{\Upsilon}$ with $\boldsymbol{\mathcal{D}} := \big[\ \boldsymbol{\mathcal{D}}_1, \dots, \boldsymbol{\mathcal{D}}_n, \dots, \boldsymbol{\mathcal{D}}_h\ \big] \in \mathbb{R}^{k\times h}$ $(\boldsymbol{\mathcal{D}}_n \in \mathbb{R}^k, n \in \mathbb{H})$, so that Eqs. (19) and (20) can be combined as

$$\boldsymbol{V}(t) := \boldsymbol{\mathcal{V}}(t) + \boldsymbol{\mathcal{D}}\boldsymbol{\mathcal{X}}(t). \tag{21}$$

To expand Eq. (21) in the temporal direction considering the planning time-horizon $[0, T]$, the vectors $\boldsymbol{V}$ and $\boldsymbol{\mathcal{V}}$ are defined as $\boldsymbol{V} := \big[\ \boldsymbol{V}(1)^\top, \dots, \boldsymbol{V}(t)^\top, \dots, \boldsymbol{V}(\ell)^\top\ \big]^\top \in \mathbb{R}^{k\ell}$ and $\boldsymbol{\mathcal{V}} := \big[\ \boldsymbol{\mathcal{V}}(1)^\top, \dots, \boldsymbol{\mathcal{V}}(t)^\top, \dots, \boldsymbol{\mathcal{V}}(\ell)^\top\ \big]^\top \in \mathbb{R}^{k\ell}$. Then, the squared voltage magnitudes of all nodes $g \in \mathbb{V}$ across all time-intervals $t \in \mathbb{S}$, is succinctly defined by

$$\boldsymbol{V} := \boldsymbol{\mathcal{V}} + \sum_{n=1}^{h} \overline{\boldsymbol{\mathcal{D}}}_n \boldsymbol{x}_n \tag{22}$$

where $\overline{\boldsymbol{D}}_n := \boldsymbol{D}_n \oplus \cdots \oplus \boldsymbol{D}_n \oplus \boldsymbol{D}_n \in \mathbb{R}^{k\ell\times\ell}$ (ℓ times execution of $\oplus$ operation) for all $n \in \mathbb{H}$. Lastly, a network constraint is introduced to maintain all nodal voltages within the operational range $[\underline{v}, \overline{v}]$, where $\underline{v} \in \mathbb{R}$ and $\overline{v} \in \mathbb{R}$ are the lower and upper bounds on voltage magnitude, respectively. Using Eq. (22), the corresponding *voltage constraint* can be written as

$$\underline{v}^2\mathbf{1} \le \boldsymbol{\mathcal{V}} + \sum_{n=1}^{h} \overline{\boldsymbol{D}}_n \boldsymbol{x}_n \le \overline{v}^2\mathbf{1}, \tag{23}$$

where $\mathbf{1} \in \mathbb{R}^{k\ell}$. Importantly, the voltage constraint (23) is coupled by the battery profiles $\boldsymbol{x}_n$ of all EVs that are connected from various locations of the distribution feeder.

With the above as background, this paper seeks to minimize the operational costs that are incurred by all EV customers $n \in \mathbb{H}$ over the planning time-horizon $[0, T]$, where the operational cost corresponding to customer $n \in \mathbb{H}$, denoted by $\Omega_n(\boldsymbol{x}_n)$, is defined in (8). Hence, the optimization problem is to minimize

$$\sum_{n\in\mathbb{H}} \Omega_n(\boldsymbol{x}_n) := \sum_{n=1}^{h}\Big(\sum_{t=1}^{\ell}\big(\Delta\eta(t)x_n(t) + \alpha_n x_n(t)^2\big)\Big), \tag{24}$$

subject to voltage constraint (23) and individual EV constraints in QP-1. The following lemma expresses the respective constrained minimization problem as a centralized QP.

Lemma 2 (*QP-2*). *The minimization of operational costs of all EV customers in expression (24), subject to the voltage constraint (23) and each EV-specific battery constraints (9b)–(9c), can be succinctly written as the following centralized QP:*

$$\min_{\mathbf{X}\in\mathbb{R}^{\ell h}} \mathbf{X}^\top\mathbf{H}\mathbf{X} + \mathbf{C}^\top\mathbf{X} \tag{25a}$$

subject to

$$\boldsymbol{\mathcal{A}}_1\mathbf{X} \ge \boldsymbol{\mathcal{B}}_1 \tag{25b}$$

$$\boldsymbol{\mathcal{A}}_2\mathbf{X} = \boldsymbol{\mathcal{B}}_2 \tag{25c}$$

where

$$\begin{aligned}
\mathbf{X} &:= \left[\, \boldsymbol{x}_1^\top, \ldots, \boldsymbol{x}_n^\top, \ldots, \boldsymbol{x}_h^\top \,\right]^\top && \in \mathbb{R}^{\ell h},\\
\mathbf{H} &:= \oplus_{n=1}^{h} \boldsymbol{H}_n && \in \mathbb{R}^{\ell h\times\ell h},\\
\mathbf{C} &:= \left[\, \boldsymbol{c}^\top, \ldots, \boldsymbol{c}^\top, \ldots, \boldsymbol{c}^\top \,\right]^\top && \in \mathbb{R}^{\ell h},\\
\boldsymbol{\mathcal{A}}_1 &:= \left[\, \mathbb{A}^\top \quad \mathbb{D}^\top \quad -\mathbb{D}^\top \,\right]^\top && \in \mathbb{R}^{(4\ell h+2k\ell)\times\ell h},\\
\mathbb{A} &:= \oplus_{n=1}^{h} \boldsymbol{A}_n && \in \mathbb{R}^{4\ell h\times\ell h},\\
\mathbb{D} &:= \left[\, \overline{\boldsymbol{D}}_1, \ldots, \overline{\boldsymbol{D}}_n, \ldots, \overline{\boldsymbol{D}}_h \,\right] && \in \mathbb{R}^{k\ell\times\ell h},\\
\boldsymbol{\mathcal{B}}_1 &:= \left[\, \mathbf{u}^\top \quad \underline{\boldsymbol{w}}^\top \quad \overline{\boldsymbol{w}}^\top \,\right] && \in \mathbb{R}^{(4\ell h+2k\ell)},\\
\mathbf{u} &:= \left[\, \boldsymbol{b}_1^\top, \ldots, \boldsymbol{b}_n^\top, \ldots, \boldsymbol{b}_h^\top \,\right]^\top && \in \mathbb{R}^{4\ell h},\\
\underline{\boldsymbol{w}} &:= \underline{v}^2\mathbf{1} - \boldsymbol{\mathcal{V}} && \in \mathbb{R}^{k\ell},\\
\overline{\boldsymbol{w}} &:= -\overline{v}^2\mathbf{1} + \boldsymbol{\mathcal{V}} && \in \mathbb{R}^{k\ell},\\
\boldsymbol{\mathcal{A}}_2 &:= \oplus_{n=1}^{h} \bar{\boldsymbol{A}}_n && \in \mathbb{R}^{4\ell h\times\ell h},\\
\boldsymbol{\mathcal{B}}_2 &:= \left[\, \bar{\boldsymbol{b}}_1^\top, \ldots, \bar{\boldsymbol{b}}_n^\top, \ldots, \bar{\boldsymbol{b}}_h^\top \,\right]^\top && \in \mathbb{R}^{4\ell h}
\end{aligned}$$

and $\boldsymbol{x}_n$, $\boldsymbol{H}_n$, $\boldsymbol{A}_n$, $\bar{\boldsymbol{A}}_n$, $\boldsymbol{b}_n$, $\bar{\boldsymbol{b}}_n$ for all $n \in \mathbb{H}$ and $\boldsymbol{c}$ are defined in QP-1.

Proof. The result directly follows from Eqs. (23), (24) and Lemma 1. The objective function (25a) minimizes the total operational cost of EV customers defined in (24). Constraint (25b) combines voltage constraint (23) and the aggregated constraint (9b) for all EVs in $\mathbb{H}$. Constraint (25c) aggregates constraint (9c) for all EVs in $\mathbb{H}$. ■

In the proposed implementation, a CO solves QP-2 and notifies the resultant EV battery profile $\boldsymbol{x}_n$ to each EV customer $n \in \mathbb{H}$. Throughout, the process of an EV customer $n \in \mathbb{H}_1$ implementing the CO-specified battery profile obtained from QP-2 is referred to as *Network-aware EV Charging-Discharging (N-EVCD)*, and the process of an EV customer $n \in \mathbb{H}_2$ implementing the CO-specified battery profile obtained from QP-2 is referred to as simply *Network-aware EV Charging (N-EVC)*.

For ease of reference, key notation introduced in the preceding text are summarized in Appendix.

Remark 1. While the non-linear power flow equations (e.g., DistFlow equations [37]) are more accurate, their inclusion in EV-based optimization problems with a fine time resolution and a large number of EVs makes the optimization problem presently intractable for near-real-time control applications. Thus, the LinDistFlow equations in [30] were proposed to support the formulation of mathematical optimization problems that can be solved in polynomial time to facilitate faster computations. Specifically, the LinDistFlow equations are derived from the DistFlow equations by assuming that the line losses are negligible compared to line flows. According to [30] and [39], such an approximation tends to introduce a small relative error, typically on the order of 1% [40]. A straightforward adjustment of the voltage constraint to accommodate for linearization errors caused by discarding line losses in the LinDistFlow equations is to maintain a safety buffer of 1% about the permissible voltage limits — i.e., setting the lower voltage bound to a slightly higher limit (e.g., $\underline{v} \approx 0.96$ p.u.) and the upper voltage bound to a slightly lower limit (e.g., $\overline{v} \approx 1.04$ p.u.) — with respect to a voltage delivery standard of $\pm 5\%$ about the nominal voltage.

3.4. Receding horizon optimization (RHO)-based network-aware EV battery scheduling

To accommodate EV charge requirements that are unknown to the CO ahead of EV grid-connection, and to support updates in prespecified EV departure times, a RHO-based implementation for N-EVC(D) is proposed as outlined in Algorithm 1.

Algorithm 1: Receding Horizon Optimization (RHO)-based N-EVC(D)

1 **Initialize** time-step $j = 0$ and $\ell = T/\Delta$.
2 **Repeat** at each time-step j,
3 Each newly joined $\text{EV}_n (n \in \mathbb{H})$ that arrived over the time interval $(\max\{(j-1), 0\}\Delta,\ j\Delta)$ sends their charging specification $\Lambda_n := \{a_n, d_n, \sigma_n, \hat{u}_n, \ddot{u}_n, \underline{u}_n, \overline{u}_n, \overline{x}_n, \underline{x}_n, \overline{\mu}_n, \underline{\mu}_n\}$ to the CO.
4 Each grid-connected $\text{EV}_n (n \in \mathbb{H})$ that intends to depart earlier or later than the scheduled time $[d_n\Delta|j]$ resends Λ_n to the CO, incorporating the updated index d_n. In case where an EV leaves unexpectedly, the target SoC will potentially not be adhered.
5 The CO solves QP-2 over the time window $[j\Delta, (j+\ell)\Delta]$ and yields a sequence of control actions $\boldsymbol{x}_n := \{x_n[1|j], \ldots, x_n[t|j], \ldots, x_n[\ell|j]\}$ for each grid-connected $\text{EV}_n (n \in \mathbb{H})$.
6 The CO notifies to each grid-connected $\text{EV}_n (n \in \mathbb{H})$ the charge or discharge rate to be applied, which is obtained for the first time-index of the control sequence $x_n(j) := x_n[1|j]$.
7 Each grid-connected $\text{EV}_n (n \in \mathbb{H})$ charges or discharges at a rate of $x_n(j)$ over the time interval $\big(j\Delta, (j+1)\Delta\big)$.
8 The CO estimates the battery SoC for each $\text{EV}_n (n \in \mathbb{H})$ as per the specific EV battery model.
9 The CO updates $\hat{u}_n := u_n[1|j]$ and $d_n = d_n - 1$ for each $\text{EV}_n (n \in \mathbb{H})$, in preparation for the next time-step.
10 Shift the time horizon by updating $j = j + 1$ and repeat Steps 3 - 10.

Receding horizon optimization is a real-time optimization technique that involves repeatedly solving an optimization problem over a moving time horizon. At each current time $j\Delta$, a future time window with size, say, $[j\Delta, (j+\ell)\Delta]$, is considered, and an optimal control sequence

$\boldsymbol{x}_n := \{x_n[1|j], \ldots, x_n[t|j], \ldots, x_n[\ell|j]\}$ is determined relative to the current time-step j. Here, the notation $[t|j]$ denotes prediction time-step t relative to current time-step j, as in [41]. In order to handle unexpected changes in the system after time $(j+1)\Delta$, only $x_n[1|j]$ for each $\text{EV}_n (n \in \mathbb{H})$ is applied, and the time-window is moved forward to time $(j+1)\Delta$.

In contrast to the EV scheduling methods proposed in [7–10,14,19,22], Algorithm 1 enables EVs to connect and disconnect from the grid without prior notice, leading to a more practical implementation. Algorithm 1 also supports updates in SoC estimates at each time-step in order to improve the performance of the algorithm in reaching a customer-specified target SoC ahead of the departure time. Extensions of Algorithm 1 to incorporate updates in target SoC and updates in real-time non-EV demand are straight forward.

4. Numerical simulations

In this section, the performance of the proposed EV charge–discharge scheduling method is evaluated on a modified IEEE 13 node test feeder, consistent with the approach taken in [8]. Specifically, a single-phase representation of the IEEE 13 node test feeder is adopted, in which the transformer between nodes 2 and 3, the switch between nodes 6 and 7 and all capacitor banks are discarded, as illustrated in Fig. 2.

The following numerical simulations consider EV charging and discharging of $h = 600$ customers distributed across a medium voltage distribution feeder. In particular, with reference to Fig. 2, each node, except nodes 0, 1 and 6, serves 60 customers such that $N^g = 60$ for $g \in \{2, \ldots, 5, 7, \ldots, 12\}$ and $N^g = 0$ for $g \in \{0, 1, 6\}$. At each node serving 60 EV customers, half of the customers are equipped with gridable EVs and the remainder are equipped with charge-only EVs. The customers are assigned different EV models as reported in [42], with battery capacities (c_n) lying in the range $[16, 90]$ kWh. Further, each customer is assumed to have a level-2 charger supporting a typical maximum charge rate of $\overline{x}_n = 6.6$ kW, as in [8]. For customers in $\mathbb{H}_1$, a maximum discharge rate of $\underline{x}_n = -6.6$ kW is additionally considered. The EV arrival and departure times (a_n and d_n) are reflective of survey data gathered by the Victorian Department of Transport in Australia [43], which contains individual vehicle travel records for a 24 h period. As in [8], the initial SOC of each EV $(\hat{u}_n)$ is within [0.3, 0.6] times the battery capacity — such that there is a uniform distribution across all EV initial SOC settings. Following [24], the minimum SoC $(\underline{u}_n)$ and maximum SoC $(\overline{u}_n)$ for each EV are considered as fractions of 0.2 and 0.85 of the battery capacity, respectively. The charge efficiency $(\overline{\mu}_n)$ and discharge efficiency $(\underline{\mu}_n)$ for each EV are set to 0.9 and 1.1, respectively. Further, α_n is fixed as $\alpha_n = 5 \times 10^{-4}$ \$/kW^2 for each EV.

The non-EV power consumption $(\boldsymbol{z}_n)$ for each of the $h = 600$ customers is obtained from a real dataset [44] publicly released by Ausgrid, an electricity distribution company in New South Wales, Australia [45]. The extracted data corresponds to the residential power consumption of a set of 300 residential customers on 5th July 2012, a day on which several peak demand conditions were observed. The dataset is then duplicated to populate non-EV power consumption for $h = 600$ customers across the day.

To maintain a high level of power quality throughout the medium voltage feeder, the ANSI C84.1 standard is followed with a maximum voltage threshold of 5% above the nominal voltage, and a minimum voltage threshold of 5% below the nominal voltage, i.e., $\underline{v} = 0.95$ p.u. and $\overline{v} = 1.05$ p.u.

As illustrated in Fig. 3, a ToU financial policy is considered as employed by the AGL Energy, an energy provider in Australia [46]. All simulations are conducted in Python 3.8.2 + CVXPY [47] on a MacBook Pro with Intel Core i5 and 8 GB memory.

In the numerical simulations that follow, two *simulation settings* are considered: *Setting 1* has a heterogeneous load arrangement wherein customers $n \in \mathbb{H}$ are assigned with heterogeneous non-EV load profiles and heterogeneous EV arrival-departure times — all consistent with the descriptions above. By contrast, *Setting 2* consists of a homogeneous load arrangement wherein all customers $n \in \mathbb{H}$ have the same non-EV demand profile $\boldsymbol{z}_n$ and the same EV charging specification given by $\Lambda_n := \{a_n : 10, d_n : 41, c_n : 75, \hat{u}_n : 40, \ddot{u}_n : 64, \underline{u}_n : 15, \overline{u}_n : 64, \overline{x}_n : 6.6, \underline{x}_n : -6.6, \overline{\mu}_n : 0.9, \underline{\mu}_n : 1.1\}$.

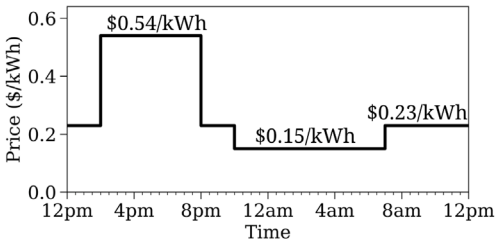

Fig. 3. Pricing profile $\boldsymbol{\eta}$ where the *off-peak* period is from 10 pm – 7 am, the *shoulder-peak period* is from 7 am – 2 pm and 8 pm – 10 pm, and the *peak* period is from 2 pm – 8 pm.

Table 1
Simulation scenarios.

	Scenario 1	Scenario 2	Scenario 3
Simulation setting	Setting 1	Setting 1	Setting 2
Implementation by EVs in $\mathbb{H}_1$ (gridable EVs)	P-EVCD	N-EVCD	N-EVCD
Implementation by EVs in $\mathbb{H}_2$ (charge-only EVs)	P-EVC	N-EVC	N-EVC

4.1. Assessing the benefit of N-EVC(D)

In this section, simulation settings 1 and 2 are incorporated into three *Simulation Scenarios*, as outlined in Table 1. Fig. 4 presents the power flow profiles and nodal voltage profiles corresponding to each of the three scenarios in Table 1.

For each scenario in Table 1, Fig. 4(a,c,e) presents the sum of non-EV load profiles $\boldsymbol{z}_n$ of all customers $n \in \mathbb{H}$ defined by $\sum_n \boldsymbol{z}_n$, the sum of EV battery profiles $\boldsymbol{x}_n$ of all customers $n \in \mathbb{H}$ defined by $\sum_n \boldsymbol{x}_n$, and the sum of grid power profiles $\boldsymbol{y}_n$ of all customers $n \in \mathbb{H}$ defined by $\sum_n \boldsymbol{y}_n$. Throughout, $\sum_n \boldsymbol{z}_n$ is referred to as the *aggregate non-EV load profile*, $\sum_n \boldsymbol{x}_n$ is referred to as the *aggregate battery profile*, and $\sum_n \boldsymbol{y}_n$ is referred to as the *aggregate grid power profile*. As illustrated in Fig. 4(a,c,e), the aggregate non-EV load profile $(\sum_n \boldsymbol{z}_n)$ rises to its peak during the peak-pricing period and then gradually declines through the shoulder-pricing period to the off-peak-pricing period, consistent with the pricing profile $\boldsymbol{\eta}$ in Fig. 3.

For each scenario in Table 1, Fig. 4(b,d,f) presents the *baseline voltage profiles* denoted by $\boldsymbol{\mathcal{V}}^{\frac{1}{2}} \in \mathbb{R}^{k\ell}$ and the *resultant nodal voltage profiles* denoted by $\boldsymbol{V}^{\frac{1}{2}} \in \mathbb{R}^{k\ell}$, where $\boldsymbol{\mathcal{V}}$ and $\boldsymbol{V}$ were previously defined in Eq. (22). Recall, the baseline voltage profiles $\boldsymbol{\mathcal{V}}^{\frac{1}{2}}$ are attributed to the non-EV load, whereas the resultant nodal voltage profiles $\boldsymbol{V}^{\frac{1}{2}}$ are attributed to the total load (EV and non-EV load). In a special case where none of the EVs are connected to the distribution network, the resultant nodal voltage profiles reduce to the baseline voltage profiles, i.e., $\boldsymbol{V}^{\frac{1}{2}} = \boldsymbol{\mathcal{V}}^{\frac{1}{2}}$. Each of the nodal voltage profiles in Fig. 4(b,d,f) are grouped into four clusters, that by inspection, exhibited similar voltage variations. Cluster 1 consists of nodes 2, 3, 4, 5, Cluster 2 consists of nodes 7, 8, 12, Cluster 3 consists of nodes 9, 10, and Cluster 4 consists of node 11. Geographically, Cluster 1 contains nodes that are located closer to the feeder head, followed by nodes in clusters 2, 3 and 4, respectively. The envelopes enclosing the respective nodal voltage profiles corresponding to each cluster are presented in Fig. 4(b,d,f), with dashed lines representing the baseline voltage profiles $\boldsymbol{\mathcal{V}}^{\frac{1}{2}}$ and solid lines representing the resultant voltage profiles $\boldsymbol{V}^{\frac{1}{2}}$.

Fig. 4(a–b) considers Scenario 1, where the process of EV charging and discharging is coordinated via P-EVC(D). Recall, P-EVC(D)

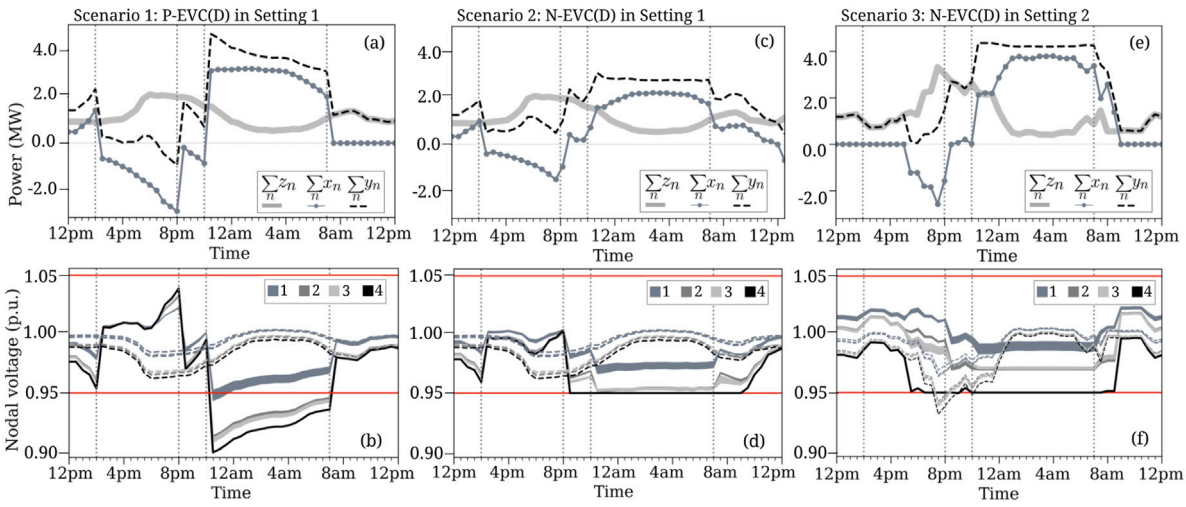

Fig. 4. (a,c,e): The aggregate non-EV load profile ($\sum_n z_n$), the aggregate battery profile ($\sum_n x_n$), the aggregate grid power profile ($\sum_n y_n$), and **(b,d,f)**: the nodal voltage profiles, corresponding to each scenario in Table 1. In Figs (b,d,f), the dashed curves represent the envelopes of baseline voltage profiles (considering only the non-EV load), $\mathcal{V}^{\frac{1}{2}}$, and the solid curves represent the envelopes of resultant nodal voltage profiles (considering both EV and non-EV load), $\boldsymbol{V}^{\frac{1}{2}}$. The envelopes in different colors correspond to different node clusters shown in the figure legend: Cluster 1 (nodes 2,3,4,5), Cluster 2 (nodes 7, 8, 12), Cluster 3 (nodes 9, 10) and Cluster 4 (node 11). The red lines mark the upper and lower voltage boundaries.

implements the solution to QP-1 that is defined in Lemma 1. It can be clearly observed that the aggregate grid power profile in Fig. 4(a) has two prominent peaks — at 2 pm and 10.30 pm — which are 2.54 times and 2.98 times greater than the corresponding aggregate non-EV load ($\sum_n \boldsymbol{z}_n$) at those times, respectively. In Fig. 4(a), the aggregate grid power profile ($\sum_n \boldsymbol{y}_n$) is negative at certain time points in the peak period and positive at all other times. At times when it is negative (i.e., when $\sum_n \boldsymbol{y}_n(t) < 0$), the gridable EVs discharge to support the non-EV demand and deliver surplus energy back to the grid. To get prepared for discharge operations taking place in the peak pricing period, the gridable EVs (particularly with lower SoCs) fill their batteries as much as possible ahead of the peak-pricing period, which results in a short charging period from 12 – 2 pm in the shoulder-peak period. The aggregate battery profile ($\sum_n \boldsymbol{x}_n$) continues to rise from 12 – 2 pm (leading to the load peak at 2 pm) as more and more gridable EVs become available for charging. During the peak pricing period, the gridable EVs contribute to peak-curtailment via V2G and thereby improve their operational savings. The highest load peak in the off-peak pricing period (at 10.30 pm) is formed when all gridable and charge-only EVs commence charging to satisfy their charge requirements. In Fig. 4(b), the envelopes of baseline voltage profiles, $\mathcal{V}^{\frac{1}{2}}$, for each of the four clusters, are within ±5% of the nominal voltage. However, the envelopes of resultant voltage profiles arising from P-EVC(D), $\boldsymbol{V}^{\frac{1}{2}}$, are below 5% of the nominal voltage in all clusters.

Fig. 4(c–d) considers Scenario 2, where the process of EV charging and discharging is coordinated via N-EVC(D), which is implemented along with RHO as outlined in Algorithm 1. Recall, N-EVC(D) implements the solution to QP-2 in Lemma 2. Since both scenarios 1 and 2 are based on simulation Setting 1, the aggregate non-EV load profiles ($\sum_n \boldsymbol{z}_n$) in Fig. 4(a) and Fig. 4(c) are identical. However, the aggregate grid power profile ($\sum_n \boldsymbol{y}_n$) in Fig. 4(c) is flatter (less prominent peaks and valleys) when compared to Fig. 4(a). More specifically, the aggregate grid power profile obtained from N-EVC(D) in Fig. 4(c) has a peak of 3.02 MW at 10.30 pm, which is 36% less than the highest load peak observed with P-EVC(D) in Fig. 4(a). Such a peak load reduction with N-EVC(D) is obtained because QP-2 includes a voltage constraint which restricts EVs to charge and discharge at lower magnitudes in order to avoid extensive voltage deviations. As shown in Fig. 4(d), N-EVC(D) maintains voltages across all nodes to stay within the upper and lower limit of ±5% of the nominal voltage. Although voltage rise above 5% of the nominal voltage is not observed in any of the four clusters with either P-EVC(D) in Fig. 4(b) or N-EVC(D) in Fig. 4(d), the voltage rise is considerably reduced with N-EVC(D) when compared to P-EVC(D).

It is worth noting that the computational time required to solve QP-1 for each EV_n in Scenario 1 is, on average, 53 milliseconds, with the CVXPY Python solver. The coupled voltage constraint (23) adds an additional level of complexity, which requires, on average, 36 seconds to solve QP-2 on each time-step of the receding time horizon in Scenario 2.[1]

Fig. 4(e–f) demonstrates the results for Scenario 3, which implements RHO-based N-EVC(D) considering a simulation setting where all customers have the same non-EV load profile $\boldsymbol{z}_n$ and the same EV charging specification Λ_n, as per Setting 2. In other words, it is considered that all customers in Scenario 3 have the same trend in non-EV power consumption, the same EV charge requirement and the same time duration available for charging the EVs. Despite such similarities, the envelopes of baseline voltage profiles resulting from the non-EV load, $\mathcal{V}^{\frac{1}{2}}$, and the envelopes of nodal voltage profiles resulting from the total load, $\boldsymbol{V}^{\frac{1}{2}}$, are different across various clusters of nodes, as seen in Fig. 4(f). In Fig. 4(e), the aggregate non-EV load profile ($\sum_n \boldsymbol{z}_n$) peaks at 7.30 pm, with a more pronounced peak than the aggregate non-EV load peak observed in Fig. 4(a) or Fig. 4(c). Consequently, the envelopes of baseline voltage profiles, $\mathcal{V}^{\frac{1}{2}}$, for clusters 3 and 4 are below 0.95 p.u. from 7 – 9 pm, as shown in Fig. 4(f). By contrast, the envelopes of voltage profiles arising from N-EVC(D), $\boldsymbol{V}^{\frac{1}{2}}$, are within the acceptable ±5% threshold, for all clusters. Thus, N-EVC(D) corrects the observed baseline voltage violation (caused by the non-EV load), eventually improving the power quality across the test feeder.

In Fig. 4(b,d,f), the voltage profile of node 11 (Cluster 4) is more frequently the closest to the upper and lower voltage boundaries. Hence, voltage constraint at node 11 is more likely to be binding. Conceptually, node 11 is the furthest from the feeder head in terms of line impedance, and therefore the voltage at node 11 is impacted by the power consumption (and injection) of EV and non-EV loads connected to all nodes of the distribution feeder.

[1] The computational time required to solve QP-2 involving 6000 EVs is, on average, 48 seconds.

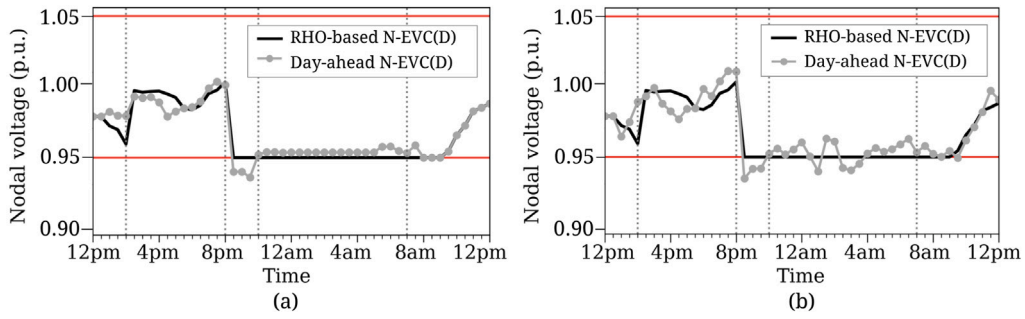

Fig. 5. The voltage profile of node 11 when N-EVC(D) is implemented with RHO (RHO-based N-EVC(D) as per Algorithm 1) and without RHO (day-ahead N-EVCD). Fig. 5(a) considers the case where day-ahead estimated EV arrival times are different from actual EV arrival times, and Fig. 5(b) additionally considers the case where day-ahead forecasted non-EV load is different from actual non-EV load.

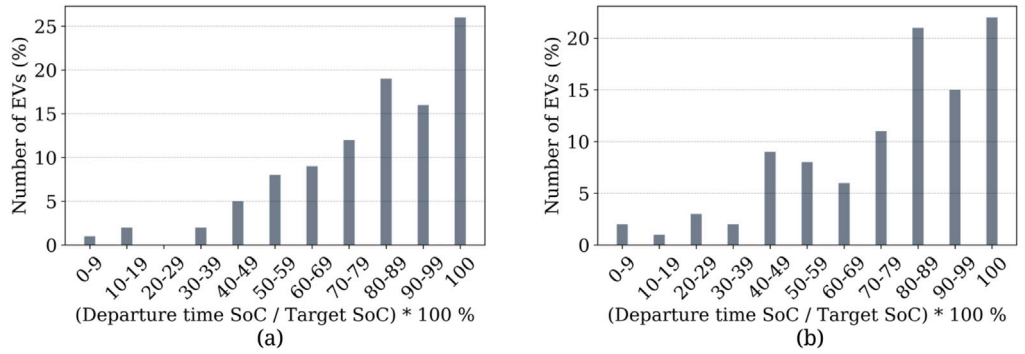

Fig. 6. The departure time SoC as a percentage of the target SoC when N-EVC(D) is implemented in the day-ahead (i.e., without RHO).

4.2. Assessing the benefit of RHO-based N-EVC(D)

In this section, the benefits of RHO-based N-EVC(D) are assessed by considering the impact of non-deterministic EV arrival times and uncertain non-EV load. For this simulation, actual arrival times of EVs a_n and actual non-EV load of customers $\boldsymbol{z}_n$ are considered as per Setting 1. The methodology employed in [41] is used to emulate the day-ahead arrival time for each EV_n, denoted by $\hat{a}_n$, and the day-ahead non-EV load profile for each customer $n \in \mathbb{H}$, denoted by $\hat{\boldsymbol{z}}_n$. In more detail, the day-ahead arrival time for each EV_n is emulated by including uncertainty as $\hat{a}_n := a_n + \delta$, where δ is a random number generated from a normal distribution of mean zero with a standard deviation of 20% about actual arrival time a_n. Moreover, the day-ahead non-EV load forecast for each customer $n \in \mathbb{H}$ is emulated by including uncertainty as $\hat{z}_n(t) = z_n(t) + \epsilon(t)$ for all $t \in \mathbb{S}$, where $\epsilon(t)$ is a random number generated from a normal distribution of mean zero with a standard deviation of 20% of $z_n(t)$. Here, the standard deviation of 20% is consistent with the approach in [41].

Fig. 5 depicts the nodal voltage profile of node 11 (Cluster 4) when N-EVC(D) is implemented with RHO (*RHO-based N-EVC(D)*) and without RHO (*day-ahead N-EVC(D)*) for two important cases, where Fig. 5(a) includes the uncertainty of EV arrival times and Fig. 5(b) includes the uncertainty of non-EV load in addition to the uncertainty of EV arrival times. While the day-ahead N-EVC(D) method implements EV charge-discharge profiles that are determined a day-ahead using various types of estimated and forecasted data, the RHO-based N-EVC(D) method continuously updates EV charge-discharge profiles in near-real-time to address various forms of uncertainties. In Fig. 5(a), it is seen that the nodal voltage profile with day-ahead N-EVC(D) is different from the nodal voltage profile with RHO-based N-EVC(D) due to the slight differences between actual EV arrival times (a_n) and estimated EV arrival times ($\hat{a}_n$). Further, it is observed that implementing N-EVC(D) without RHO results in under-voltage conditions between 8.30 pm to 10 pm. From Fig. 5(b), it is inferred that when uncertainty of non-EV load is combined with uncertainty of EV arrival times, the day-ahead N-EVC(D) method aggravates violations of the voltage constraint. By contrast, implementing RHO-based N-EVC(D) improves supply voltages with no voltage excursions observed in either Fig. 5(a) or Fig. 5(b). It is worth mentioning that RHO-based N-EVC(D) accommodates incoming EVs without any prior notice and supports near real-time updates in non-EV demand forecasts — all of which enable greater preservation of the voltage constraint as observed in Fig. 5(a) and Fig. 5(b).

Fig. 6(a) and Fig. 6(b) report the departure time SoC of each EV when they follow battery profiles computed by the day-ahead N-EVC(D) method in Fig. 5(a) and Fig. 5(b), respectively. It is seen from Fig. 6(a) and Fig. 6(b) that only a portion of EVs (26% and 22%) reach their target SoC ($\ddot{u}_n$) completely. Moreover, the SoC on departure for 10% of EVs in Fig. 6(a) and 17% of EVs in Fig. 6(b) is less than half of their target SoC. Conversely, when RHO-based N-EVC(D) is implemented as in Fig. 5(a) and Fig. 5(b), all EVs attain their target SoC ahead of the departure time.

From the results presented in Figs. 5 and 6, it can be deduced that the N-EVC(D) method must be combined with RHO, in order to satisfy both the required distribution network voltage delivery requirements and the EV customer charge preferences.

4.3. Assessing the customer benefit

In this section, a set of customers, one from each node, is carefully selected to quantify operational costs for EV charging and discharging. For the purpose of comparison, Setting 2 is specifically chosen, such that the EV charging specification Λ_n and the non-EV load profile $\boldsymbol{z}_n$ remain the same for all customers. For each customer $n \in \mathbb{H}$ picked from each node $g \in \mathbb{V}$, Fig. 7 presents the operational cost ($\Omega_n(\boldsymbol{x}_n)$)

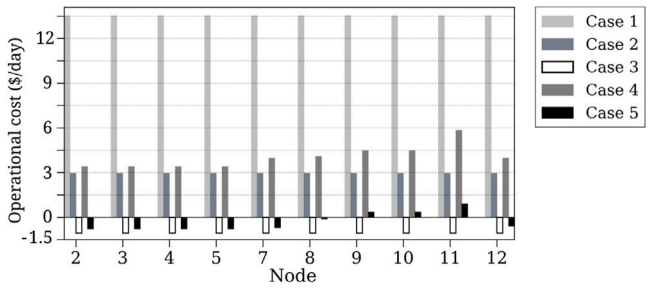

Fig. 7. Operational costs $\Omega_n(\boldsymbol{x}_n)$ attributed to a set of customers selected from each node in the distribution test feeder.

pertaining to 5 cases of EV charging, namely, **Case 1**: uncoordinated EV charging, **Case 2**: P-EVC, **Case 3**: P-EVCD, **Case 4**: N-EVC and **Case 5**: N-EVCD.

For Case 1 with uncoordinated EV charging, each $\text{EV}_n (n \in \mathbb{H})$ commences charging at full power $\overline{x}_n$ immediately upon arrival and continues charging at the same rate of $\overline{x}_n$ until the battery is charged up to the target SoC $\ddot{u}_n$. According to Fig. 7, the largest operational cost for each customer corresponds to Case 1 (uncoordinated EV charging) — where no optimization-based method is applied for EV charging. By contrast, the lowest operational cost (or rather the greatest operational saving) for each customer corresponds to Case 3 (P-EVCD) where V2G is enabled, followed by Case 2 (P-EVC) where V2G is disabled.

In cases 1–3 where network voltage conditions are excluded, each customer receives an identical EV battery profile, and as such, the operational cost stays the same for each customer across the test feeder. In cases 4 and 5, the operational costs vary across customers as a result of the network voltage constraint. In particular, the operational costs in Case 4 (N-EVC) are greater than Case 2 (P-EVC), and the operational costs in Case 5 (N-EVCD) are greater than Case 3 (P-EVCD), implying that addressing the voltage constraint potentially leads to an increase in operational costs for the customers. Specifically, customers located at nodes with a larger line impedance (e.g., nodes in clusters 3 and 4) incur larger increases in operational costs. In both cases 4 and 5, the customer at node 11 incurs the largest operational cost. It can also be observed that in Case 5 (N-EVCD), customers closer to the feeder head accrue operational benefits ($\Omega_n(\boldsymbol{x}_n) < 0$), whereas customers located far from the feeder head accrue operational costs ($\Omega_n(\boldsymbol{x}_n) > 0$). Nevertheless, all customers partaking in either Case 4 or 5 (proposed N-EVC(D) method) receive an operational cost reduction of 92% – 111% (latter corresponds to a 11% gain) when compared to uncoordinated EV charging.

4.4. Discussion

In summary, key findings from the numerical simulations are listed as follows.

- P-EVC(D) yields lower operational costs (or greater operational savings) compared to uncoordinated EV charging and N-EVC(D); however, P-EVC(D) exacerbates voltage variability, which leads to voltage violations across a distribution feeder, particularly at nodes in the extremity of the feeder.
- The requirement to address voltage constraint in N-EVC(D) potentially leads to an increase in operational costs compared to P-EVC(D). However, N-EVC(D) yields significantly lower operational costs compared to uncoordinated EV charging and it also improves supply voltages without requiring protection schemes to correct for any potential voltage violation. Protection schemes that disconnect EV charging infrastructure to correct for sustained voltage excursions would adversely impact the EV customer both financially and in terms of meeting their exact charge requirements.
- To mitigate large voltage fluctuations, N-EVC(D) returns comparatively higher charge rates to EVs located closer to the feeder head and lower charge rates to EVs located closer to the feeder extremities.
- Even if all customers and their EVs have the same non-EV load profile and the same EV specification, the charge-discharge profiles obtained from N-EVC(D) are different across the customers, resulting in different operational costs.
- In the absence of advanced knowledge of exact EV arrival times and non-EV load profiles, RHO based N-EVC(D) as opposed to day-ahead N-EVC(D) allows for considerable improvements in voltage regulation in addition to achieving the customer-specified target SoC ahead of EV departure.

In future work, the numerical simulations will be extended to investigate voltage variability of unbalanced distribution grids when supplemented with rooftop PV power generation. Future work will also explore extensions of N-EVC(D) to incorporate dynamic distribution grid constraints such as thermal network constraints. Furthermore, it is envisioned that RHO based N-EVC(D), when combined with distributed algorithms (facilitating distributed computations by EVs), will potentially reduce the computational complexity associated with solving QP-2.

5. Conclusion

This paper presented an Electric Vehicle (EV) battery scheduling method called N-EVC(D) for coordinating EV charge (and discharge) rates to improve supply voltages along a distribution feeder. The optimization problem for N-EVC(D) was posed as a quadratic program, with an objective function to minimize operational costs associated with EV charging (and discharging) in accordance with a time-of-use net metering financial policy. A coupled voltage constraint was included in the quadratic program to alleviate non-compliant voltage excursions outside the operational limits of the distribution network. A receding horizon optimization-based N-EVC(D) algorithm was also proposed to accommodate various sources of uncertainties including unexpected EV arrival and departure times. Through numerical simulations, it was demonstrated that N-EVC(D) achieved an operational cost reduction of 92% – 111% compared to uncoordinated EV charging. N-EVC(D) also achieved a peak load reduction of 36% compared to a benchmark method that omitted voltage constraints when minimizing EV operational costs. Furthermore, the receding horizon optimization-based N-EVC(D) method improved supply voltages in cases of unexpected EV arrival times and non-EV load forecast errors. Importantly, the receding horizon optimization-based N-EVC(D) method outperformed the day-ahead N-EVC(D) method with all EVs attaining their target state of charge ahead of departure.

CRediT authorship contribution statement

Nanduni I. Nimalsiri: Conceptualization, Methodology, Software, Validation, Formal analysis, Investigation, Data curation, Writing - original draft, Writing - review & editing, Visualization, Project administration. **Elizabeth L. Ratnam:** Conceptualization, Methodology, Validation, Formal analysis, Investigation, Writing - review & editing, Visualization, Supervision, Project administration. **Chathurika P. Mediwaththe:** Conceptualization, Methodology, Validation, Formal analysis, Investigation, Writing - review & editing, Visualization, Supervision, Project administration. **David B. Smith:** Conceptualization, Methodology, Validation, Formal analysis, Investigation, Writing - review & editing, Visualization, Supervision, Project administration. **Saman K. Halgamuge:** Conceptualization, Validation, Formal analysis, Investigation, Writing - review & editing, Visualization, Supervision, Project administration.

Declaration of competing interest

The authors declare that they have no known competing financial interests or personal relationships that could have appeared to influence the work reported in this paper.

Acknowledgment

Nanduni I. Nimalsiri acknowledges the financial support of an Australian National University (ANU) Postgraduate Research Scholarship and a CSIRO Data61 PhD Scholarship.

Appendix

A summary of key notation used in the problem formulation:

t	Time index	n	Customer index
$\mathbb{S}$	Set of time indices	ℓ	Number of time indices in $\mathbb{S}$
$[0,T]$	Time horizon under consideration (h)	Δ	Length of a time interval (h)
$\mathbb{H}$	Set of customers	h	Number of customers in $\mathbb{H}$
$\mathbb{H}_1$	Set of customers with gridable EVs	$\mathbb{H}_2$	Set of customers with charge-only EVs
$\eta(t)$	Price of electricity over the period $\big((t-1)\Delta, t\Delta\big)$ ($/kWh)	$\boldsymbol{\eta}$	Pricing profile

A summary of key notation specific to $\mathbf{EV}_n$ ($n \in \mathbb{H}$):

a_n	Arrival time index	d_n	Intended departure time index
$\hat{u}_n$	Initial SoC (kWh)	$\ddot{u}_n$	Target SoC (kWh)
$\overline{x}_n$	Maximum charge rate (kW)	$\underline{x}_n$	Maximum discharge rate (kW)
σ_n	Battery capacity (kWh)	α_n	Battery degradation constant ($/kW^2)
$u_n(t)$	SoC at time $t\Delta$ (kWh)	$\boldsymbol{u}_n$	SoC profile

A summary of key notation specific to customer $n \in \mathbb{H}$:

$x_n(t)$	(Dis)charge rate over the period $\big((t-1)\Delta, t\Delta\big)$ (kW)	$\boldsymbol{x}_n$	Battery profile
$z_n(t)$	Non-EV load over the period $\big((t-1)\Delta, t\Delta\big)$ (kW)	$\boldsymbol{z}_n$	Non-EV load profile
$y_n(t)$	Measured power through meter M over the period $\big((t-1)\Delta, t\Delta\big)$ (kW)		
$\Omega_n(\cdot)$	Operational cost function	$\boldsymbol{y}_n$	Grid power profile

A summary of key notation specific to the distribution network model:

g	Node index	N^g	Number of customers connected to node g
$v^g(t)$	Voltage at node g at time $t\Delta$ (p.u.)	v^0	Voltage at node 0 (p.u.)
$\underline{v}$	Minimum voltage magnitude (p.u.)	$\overline{v}$	Maximum voltage magnitude (p.u.)
$\mathcal{V}$	Set of nodes including node 0 (feeder head)		
$\mathbb{V}$	Set of nodes excluding node 0 (feeder head)		
(ij)	Distribution line connecting node i and node j		
$\mathcal{E}$	Set of distribution lines of the feeder		
$\mathcal{E}^g$	Set of distribution lines on the unique path from node 0 to node g		
$p^g(t), q^g(t)$	Real, reactive power consumed at node g over the period $\big((t-1)\Delta, t\Delta\big)$ (kW, kVAR)		
$\widetilde{p}^g(t), \widetilde{q}^g(t)$	Real, reactive power consumed by non-EV load at node g over the period $\big((t-1)\Delta, t\Delta\big)$		
$\widehat{p}^g(t), \widehat{q}^g(t)$	Real, reactive power consumed by EVs at node g over the period $\big((t-1)\Delta, t\Delta\big)$		

References

[1] Shareef H, Islam MM, Mohamed A. A review of the stage-of-the-art charging technologies, placement methodologies, and impacts of electric vehicles. Renew Sustain Energy Rev 2016;64:403–20.

[2] Dubey A, Santoso S. Electric vehicle charging on residential distribution systems: Impacts and mitigations. IEEE Access 2015;3:1871–93.

[3] Dong X, Mu Y, Xu X, Jia H, Wu J, Yu X, Qi Y. A charging pricing strategy of electric vehicle fast charging stations for the voltage control of electricity distribution networks. Appl Energy 2018;225:857–68.

[4] Nimalsiri NI, Mediwaththe CP, Ratnam EL, Shaw M, Smith DB, Halgamuge SK. A survey of algorithms for distributed charging control of EVs in smart grid. IEEE Trans Intell Transp Syst 2019;21:4497–515.

[5] De Hoog J, Alpcan T, Brazil M, Thomas D, Mareels I. Optimal charging of electric vehicles taking distribution network constraints into account. IEEE Trans Power Syst 2014;30:365–75.

[6] Richardson P, Flynn D, Keane A. Optimal charging of electric vehicles in low-voltage distribution systems. IEEE Trans Power Syst 2012;27:268–79.

[7] Zhan K, Hu Z, Song Y, Luo Z, Xu Z, Jia L. Coordinated electric vehicle charging strategy for optimal operation of distribution network. In *Proc. IEEE PES 3rd Innovative Smart Grid Technol.*, Europe, 2012, pp. 1–6.

[8] Liu M, Phanivong PK, Shi Y, Callaway DS. Decentralized charging control of EVs in residential distribution networks. IEEE Trans Control Syst Technol 2017;27:266–81.

[9] Huo X, Liu M. Decentralized electric vehicle charging control via a novel shrunken primal-multi-dual subgradient (SPMDS) algorithm. In *Proc. IEEE 59th Conf. Decis. Control*, 2020, pp. 1367–73.

[10] Cao C, Wu Z, Chen B. Electric vehicle–grid integration with voltage regulation in radial distribution networks. Energies 2020;13:1802.

[11] Nazarloo A, Feyzi MR, Sabahi M, Sharifian MBB. Improving voltage profile and optimal scheduling of V2G energy based on a new method. Adv Electr Comput Eng 2018;18:81–9.

[12] Richardson P, Flynn D, Keane A. Local versus centralized charging strategies for electric vehicles in low voltage distribution systems. IEEE Trans Smart Grid 2012;3:1020–8.

[13] Al-Awami AT, Sortomme E, Akhtar GMA, Faddel S. A voltage-based controller for an electric-vehicle charger. IEEE Trans Veh Technol 2015;65:4185–96.

[14] Clement-Nyns K, Haesen E, Driesen J. The impact of vehicle-to-grid on the distribution grid. Electr Power Syst Res 2011;81:185–92.

[15] Luo X, Chan KW. Real-time scheduling of electric vehicles charging in low-voltage residential distribution systems to minimise power losses and improve voltage profile. IET Gener Transm Distrib 2013;8:516–29.

[16] Lazarou S, Vita V, Christodoulou C, Ekonomou L. Calculating operational patterns for electric vehicle charging on a real distribution network based on renewables' production. Energies 2018;11:2400.

[17] Vita V, Lazarou S, Christodoulou CA, Seritan G. On the determination of meshed distribution networks operational points after reinforcement. Appl Sci 2019;9:3501.

[18] Sun W, Neumann F, Harrison GP. Robust scheduling of electric vehicle charging in LV distribution networks under uncertainty. IEEE Trans Ind Appl 2020;56:5785–95.

[19] Bharati G, Paudyal S. Coordinated control of distribution grid and electric vehicle loads. Electr Power Syst Res 2016;140:761–8.

[20] Shekari T, Golshannavaz S, Aminifar F. Techno-economic collaboration of PEV fleets in energy management of microgrids. IEEE Trans Power Syst 2016;32:3833–41.

[21] Crow ML, et al. Electric vehicle scheduling considering co-optimized customer and system objectives. IEEE Trans Sustain Energy 2017;9:410–9.

[22] Leou R-C. Optimal charging/discharging control for electric vehicles considering power system constraints and operation costs. IEEE Trans Power Syst 2015;31:1854–60.

[23] Suyono H, Rahman MT, Mokhlis H, Othman M, Illias HA, Mohamad H. Optimal scheduling of plug-in electric vehicle charging including time-of-use tariff to minimize cost and system stress. Energies 2019;12:1500.

[24] Xing H, Fu M, Lin Z, f Y. Decentralized optimal scheduling for charging and discharging of plug-in electric vehicles in smart grids. IEEE Trans Power Syst 2016;31:4118–27.

[25] Casini M, Vicino A, Zanvettor GG. A receding horizon approach to peak power minimization for EV charging stations in the presence of uncertainty. Int J Electr Power Energy Syst 2021;126:106567.

[26] Yi Z, Scoffield D, Smart J, Meintz A, Jun M, Mohanpurkar M, Medam A. A highly efficient control framework for centralized residential charging coordination of large electric vehicle populations. Int J Electr Power Energy Syst 2020;117:105661.

[27] Wang GC, Ratnam E, Haghi HV, Kleissl J. Corrective receding horizon EV charge scheduling using short-term solar forecasting. Renew Energy 2019;130:1146–58.

[28] Mediwaththe CP, Smith DB. Game-theoretic electric vehicle charging management resilient to non-ideal user behavior. IEEE Trans Intell Transp Syst 2018;19:3486–95.

[29] Ratnam EL, Weller SR, Kellett CM. Central versus localized optimization-based approaches to power management in distribution networks with residential battery storage. Int J Electr Power Energy Syst 2016;80:396–406.
[30] Baran ME, Wu FF. Network reconfiguration in distribution systems for loss reduction and load balancing. IEEE Power Eng Rev 1989;9:101–2.
[31] Nimalsiri N, Smith D, Ratnam E, Mediwaththe C, Halgamuge S. A decentralized electric vehicle charge scheduling scheme for tracking power profiles. In *Proc. IEEE PES Innovative Smart Grid Technol.*, 2020, pp. 1–5.
[32] Chang W-Y. The state of charge estimating methods for battery: A review. Int Sch Res Not 2013.
[33] Ratnam EL, Weller SR, Kellett CM. An optimization-based approach to scheduling residential battery storage with solar PV: Assessing customer benefit. Renew Energy 2015;75:123–34.
[34] Ratnam EL, Weller SR, Kellett CM. Scheduling residential battery storage with solar PV: Assessing the benefits of net metering. Appl Energy 2015;155:881–91.
[35] Rivera J, Wolfrum P, Hirche S, Goebel C, Jacobsen H-A. Alternating direction method of multipliers for decentralized electric vehicle charging control. In *Proc. IEEE 52nd Conf. Decis. Control*, 2013, pp. 6960–65.
[36] Hoke A, Brissette A, Smith K, Pratt A, Maksimovic D. Accounting for lithium-ion battery degradation in electric vehicle charging optimization. IEEE J Emerg Sel Top Power Electron 2014;2:691–700.
[37] Baran M, Wu FF. Optimal sizing of capacitors placed on a radial distribution system. IEEE Trans Power Deliv 1989;4:735–43.
[38] Mediwaththe CP, Blackhall L. Network-aware demand-side management framework with a community energy storage system considering voltage constraints. IEEE Trans Power Syst 2020.
[39] Farivar M, Chen L, Low S. Equilibrium and dynamics of local voltage control in distribution systems. In *Proc. IEEE 52nd Conf. Decis. Control*, 2013, pp. 4329–34.
[40] Lin W, Bitar E. Decentralized stochastic control of distributed energy resources. IEEE Trans Power Syst 2017;33:888–900.
[41] Ratnam EL, Weller SR. Receding horizon optimization-based approaches to managing supply voltages and power flows in a distribution grid with battery storage co-located with solar PV. Appl Energy 2018;210:1017–26.
[42] Battery University. Bu-1003: Electric vehicle (EV). 2021, https://batteryuniversity.com/learn/article/electric_vehicle_ev, (Accessed 25 Feb 2021).
[43] Victoria State Government - Department of Transport. VISTA Data and Publications; 2020, https://transport.vic.gov.au/about/data-and-research/vista/vista-data-and-publications (Accessed 1 March 2020).
[44] Ratnam EL, Weller SR, Kellett CM, Murray AT. Residential load and rooftop PV generation: an Australian distribution network dataset. Int J Sustain Energy 2017;36:787–806.
[45] Ausgrid. Solar home electricity data. 2020, https://www.ausgrid.com.au/Industry/Our-Research/Data-to-share/Solar-home-electricity-data (Accessed 1 March 2020).
[46] AGL. Standard retail contracts. 2020, https://www.agl.com.au/help/rates-contracts/standard-contracts, (Accessed 1 March 2020).
[47] Diamond S, Boyd S. CVXPY: A python-embedded modeling language for convex optimization. J Mach Learn Res 2016;17:1–5.